Physica E 42 (2010) 809–812

Contents lists available at ScienceDirect

Physica E

journal homepage: www.elsevier.com/locate/physe

Detection of spin polarization in a quantum wire

Tomohiro Otsuka *, Eisuke Abe, Yasuhiro Iye, Shingo Katsumoto

Institute for Solid State Physics, University of Tokyo, 5-1-5 Kashiwanoha, Kashiwa, Chiba 277-8581, Japan

ARTICLE INFO

Available online 27 October 2009

Keywords:
Quantum dot
Quantum wire
Spin polarization

ABSTRACT

We demonstrate detection of spin polarization in a quantum wire utilizing a side coupled quantum dot. By applying in-plane magnetic fields, spin split conducting channels are formed and produce spin polarization in the wire. The magnetic fields also create Zeeman split spin levels in the dot and these states are used as a spin polarization detector. Such kind of spin polarization detection with a side coupled quantum dot will operate even in the zero magnetic field by using two-electron singlet and triplet levels.

1. Introduction

Generation and detection of spin polarization in nonmagnetic semiconductors are the key technologies in the development of spintronics [1,2]. For the generation of spin polarization, spin filters utilizing spin–orbit interaction [3–5] are proposed [6–9]. On the other hand, for the detection, use of magnetic material as a lead is one possible method. But this encounters difficulties such as conductance mismatch between two different materials [10] and defect-induced scattering, which lead to the decrease of detection efficiency or strong back action to the target spin source. Here, we propose and demonstrate a detection method with least disturbance utilizing a side coupled quantum dot (QD) [11].

A QD is a structure which confines electrons in a small region and discretizes energy levels by size quantization [12]. The number of electrons in a QD is fixed and controlled through the single electron charging effect. These levels can be shifted by the gate voltage and show spin selectivity by the effect of exchange interaction or Zeeman splitting. In this article, we show that by using these levels as spin detectors, detection of the spin polarization in the target system is possible.

2. Detection method

To detect spin polarization in the target, we measure the tunneling from the target to the spin split levels in the QD. Let us consider the case that the level of up-spin has lower energy. When the Fermi energy of the target E_F lies between the up and down spin levels (Fig. 1(a)), only electrons with up-spin can go into the QD. The tunneling rate Γ_1 is proportional to the density of states of up-spin electrons in the target $D_\uparrow$. On the other hand, when both spin levels are below E_F (Fig. 1(b)), both $D_\uparrow$ and $D_\downarrow$ contribute to the tunneling rate Γ_2. The ratio Γ_1/Γ_2 becomes

$$\frac{\Gamma_1}{\Gamma_2} = \frac{D_\uparrow}{D_\uparrow + D_\downarrow} = \frac{1+P}{2}, \tag{1}$$

where $P=(D_\uparrow - D_\downarrow)/(D_\uparrow + D_\downarrow)$ is the spin polarization.

We adopt side coupled configuration, in which a QD is coupled to the target via a single tunneling barrier [13,14] (Fig. 1(c)), hence there is no net current between the QD and the target. In addition, the coupling is reduced to $\Gamma \sim 1$ kHz for minimizing the back action.

Here the voltage on gate P of the QD V_P is modulated by a square wave and the charge state of the QD follows the wave with the limitation of the tunneling rate. The tunneling rate is measured by observing the modulation of fringe electric field from the QD through the current of a quantum point contact (QPC) placed next to the QD [15–17]. Because the fringe field modifies the current of QPC synchronous with the square wave I_{sync}, the variation of the synchronous current ΔI_{sync} reflects the tunneling rate Γ. The relation between them is

$$\Delta I_{sync} \propto 1 - \frac{\pi^2}{\Gamma^2\tau^2 + \pi^2}, \tag{2}$$

where τ is the half period of the square wave [18].

By changing the DC offset voltage on gate P V_{PDC}, the spin split levels shift with respect to E_F (Fig. 1(d)). The gray region in the figure shows the energy window in which the shuttling of electrons between the QD and the target, and then the change of the charge state in the QD occur. When a level is above (below) this window, the level is always empty (filled). In both cases, there is no electron shuttling. Then ΔI_{sync} is observed in regions 1 and 2.

* Corresponding author. Tel./fax: +81 471363301.
E-mail address: t-otsuka@issp.u-tokyo.ac.jp (T. Otsuka).

1386-9477/$ - see front matter © 2009 Elsevier B.V. All rights reserved.
doi:10.1016/j.physe.2009.10.034

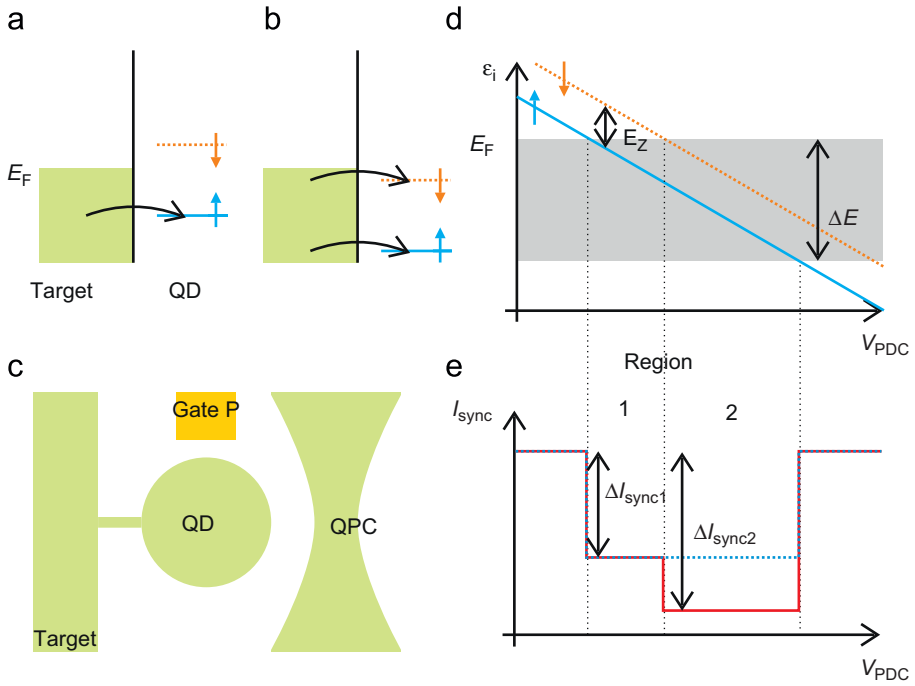

Fig. 1. (color online) (a), (b) Energy diagram when the Fermi energy of the target E_F lies between the up and down spin levels (a) and both of the levels are below E_F (b). (c) Schematic of the device structure for the detection of spin polarization. (d) Shift of spin split levels in the QD as a function of the DC voltage on gate P V_{PDC}. The gray zone shows the energy window in which electron shuttling occurs. (e) Schematic of synchronous current I_{sync} as a function of V_{PDC}. The solid (broken) line corresponds to the unpolarized (polarized) situation.

In region 1, only the up-spin level is in the window. In region 2, both of spin levels are in the window. These make difference between ΔI_{sync1} and ΔI_{sync2}, which brings the information about the polarization. In the unpolarized situation, Γ_2 is $2\Gamma_1$ and a two-step dip structure is observed (a solid line in Fig. 1(e)). In the fully polarized case, Γ_2 is same to Γ_1 and a single-step dip is formed (a broken line in Fig. 1(e)).

3. Experiment

3.1. Spin split levels in a quantum dot

First, we measure spin split levels in a QD which can be used for the spin polarization detection. Examples of such split levels are two-electron singlet–triplet spin levels in the zero magnetic field and Zeeman split levels in high magnetic fields.

The inset of Fig. 2 shows a scanning electron micrograph of the device. Au/Ti Schottky gates are deposited on the surface of a GaAs/AlGaAs two-dimensional electron gas wafer. A QD is formed by gates C, P and S, and a QPC is formed with gates S and D.

Fig. 2 shows I_{sync} as a function of V_{PDC} in the zero magnetic field. This measurement is done under the condition that the number of electrons in the QD changes between 1 and 2 with the oscillation of V_P. A two-step dip structure is clearly observed. The tunneling to the singlet level (both singlet and triplet levels) occurs in the shallow (deep) region. The width of the shallow region reflects the energy difference between singlet and triplet levels E_{ST}. We estimate E_{ST} by applying bias voltage on the target [19] as $E_{ST} = 0.6$ meV.

The Zeeman split spin levels are also observed through I_{sync} as a function of V_{PDC} with the in-plane magnetic field of $B = 14$ T (Fig. 3(a)). The number of electrons in the QD changes between 0 and 1. The region of tunneling to the up-spin level shows the shallow dip and that to both spin levels corresponds to the deep dip. Fig. 3(b) shows the magnetic field dependence of the Zeeman

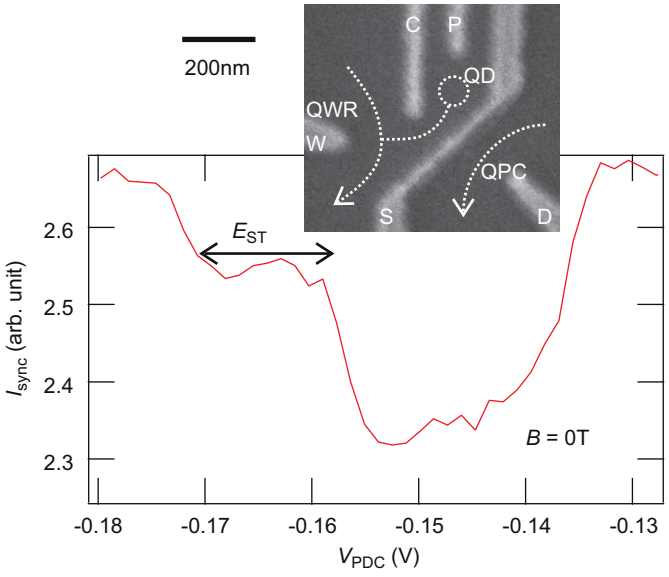

Fig. 2. (color online) Synchronous current I_{sync} as a function of the DC voltage on gate P V_{PDC} at two-electron states of the QD in the zero magnetic field. The inset shows the scanning electron micrograph of the device.

energy E_Z evaluated from the width of the shallow region. E_Z increases linearly with B and g-factor is evaluated as $|g| = 0.29$ from the slope. This value is consistent with other reports on QDs [20–22] and certifies validity of the method. Note that the electronic states in the target are also Zeeman split, but in the present experiment, the Fermi energy is set far above the spin up or down subband edges and the difference between $D_\uparrow$ and $D_\downarrow$ can be neglected.

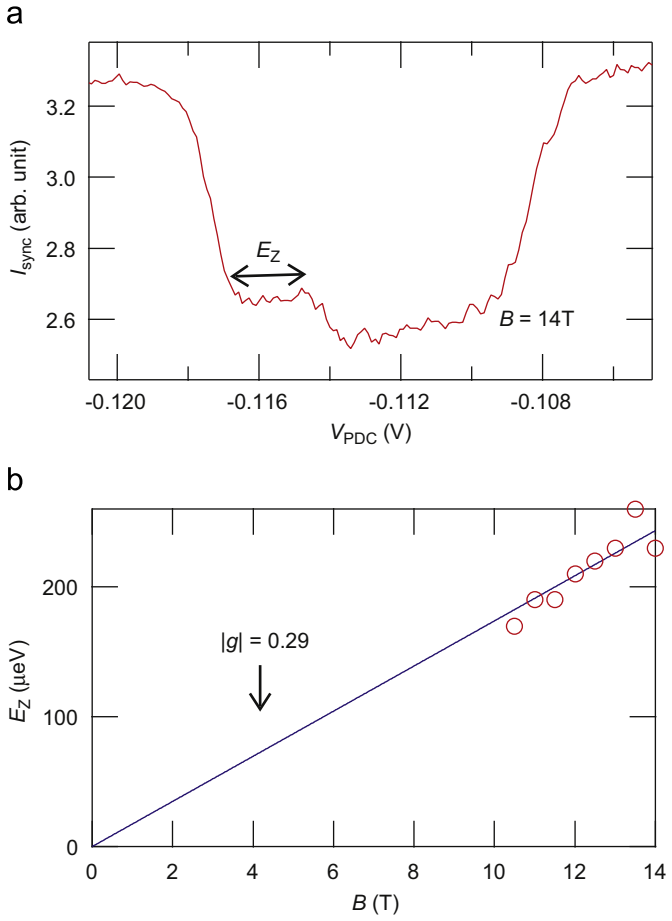

Fig. 3. (color online) (a) Synchronous current I_{sync} as a function of the DC voltage on gate P V_{PDC} at one-electron states of the QD. The in-plane magnetic field of 14 T is applied. (b) Evaluated Zeeman energy E_Z as a function of magnetic fields B (markers) and the result of fitting (a solid line).

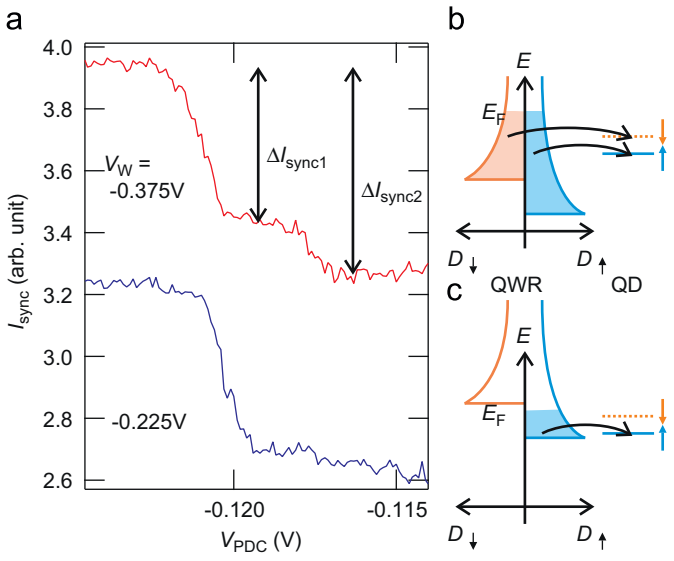

Fig. 4. (color online) (a) Synchronous current I_{sync} as a function of the DC voltage on gate P V_{PDC} with different voltages on gate W V_W. Upper (lower) corresponds to the result at $V_W = -0.375$ (−0.225) V. (b), (c) Energy diagram with the unpolarized (b) or polarized (c) quantum wire.

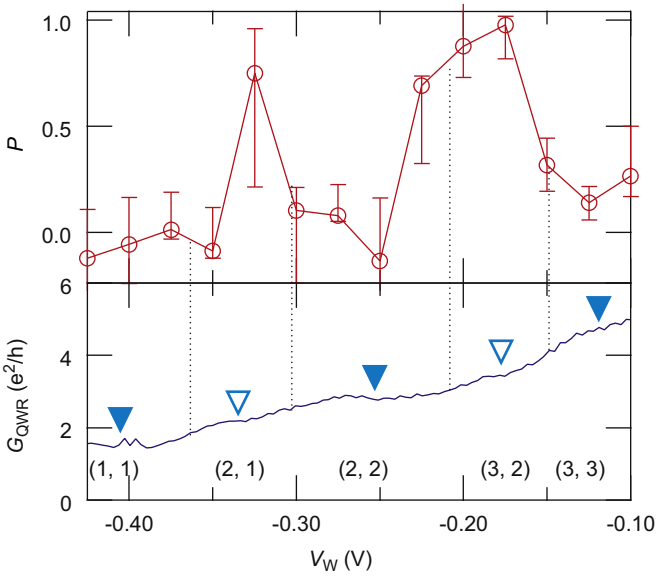

Fig. 5. (color online) Evaluated polarization P (upper) and the conductance through the QWR G_{QWR} (lower) as a function of the wire gate voltage V_W. Solid (open) triangles indicate the unpolarized (polarized) regions. Estimated number of channels with up and down spins $n_\uparrow, n_\downarrow$ are represented as $(n_\uparrow, n_\downarrow)$.

3.2. *Detection of spin polarization in a quantum wire*

Having identified the Zeeman split levels in the dot, next we demonstrate the detection of spin polarization in the target. Here we use a quantum wire (QWR) in magnetic fields as a target with controllable spin polarization. The QWR is readily formed by applying negative voltages on gate W V_W in Fig. 2. The number of conducting channels is also controlled through V_W. Because the external magnetic field splits the channels to those with different spins [23], the total spin polarization also changes with the number of channels in the QWR. This is the principle of polarization control.

The upper curve in Fig. 4(a) shows a two-step decrease of I_{sync} versus V_{PDC} at $V_W = -0.375$ V, which is similar to the result in Fig. 3(a). This manifests that both up and down spin subbands have similar density of states, namely the polarization is small (Fig. 4(b)). However, when V_W is shifted to −0.225 V as shown in the lower curve, the deep region almost disappears. This indicates that the lower spin has very low density of states in the QWR and the appearance of the spin polarization (Fig. 4(c)).

To be quantitative, we evaluated the polarization P from the depths of the two-step structure ΔI_{sync1} and ΔI_{sync2} through Eqs. (1) and (2) for different V_W and plotted the result in Fig. 5 together with the conductance through the QWR G_{QWR}. The value of P oscillates between 0 and 1. G_{QWR} shows wide plateaus (marked with solid triangles) and narrow plateaus (open triangles). The former (latter) corresponds to the spin unpolarized (polarized) situation, because the Zeeman energy is smaller than the subband energy separation of the QWR. The values of G_{QWR} at the plateaus are not the multiples of e^2/h due primarily to the complex gate configuration of this device. By comparing P and G_{QWR}, P is close to 0 around the wide plateaus in G_{QWR} and P approaches to 1 near the narrow plateaus. These results demonstrate that the side coupled QD works as a spin polarization detector.

Next we take a detailed look at the data shown in Fig. 5. There are two phenomena that cannot be explained when we interpret the results simply assuming that the QWR is long enough and all of the channels in the QWR contribute equally to the detected signal. One is the faster increase of P than G_{QWR} with increasing V_W in the wide QWR. This is explained by the difference between the point at which the polarization is detected and that at which

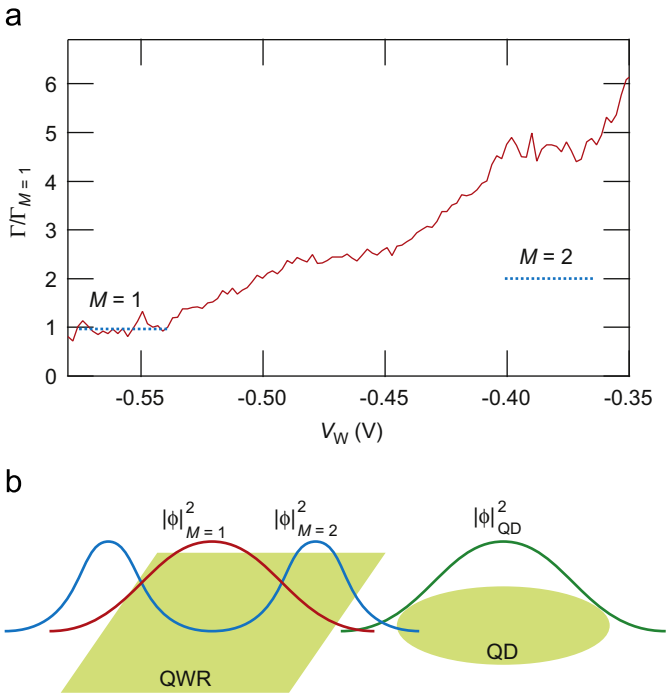

Fig. 6. (color online) (a) Effective tunneling rate Γ as a function of the wire gate voltage V_W. The value is normalized by the effective tunneling rate of the lowest ($M=1$) channel $\Gamma_{M=1}$. (b) Schematics of the wave functions ϕ in the QWR and the QD.

G_{QWR} is determined. The polarization is detected at the connection point of the QD, and G_{QWR} is defined at the narrowest point of the QWR. These points will be different in a relatively short and inhomogeneous QWR. The second is the large value of P even in the wide QWR. In the wide QWR, the contribution of the spin polarized channel decreases because the number of unpolarized channels increases. This implies that channels with larger quantum number in the QWR M have larger coupling to the QD. In this case, the observed P reflects the polarization in channels with larger M and takes a large value.

Such kind of change in the coupling strength is indeed observed. Fig. 6(a) shows Γ as a function of V_W in the zero magnetic field. Γ is normalized by the tunneling rate of the lowest ($M=1$) channel $\Gamma_{M=1}$. Γ is evaluated from ΔI_{sync} by using Eq. (2). The broken line at $M=2$ in Fig. 6(a) shows the expected value if we assume all of the channels have same coupling strength. The measured result is apparently larger than this value and the channels with larger M have larger coupling to the QD. This is the result of the spatial distribution of wave functions in the QWR, which is wider with larger M because higher energy channels feel weaker confinement. This makes larger overlap with the wave function of the QD (Fig. 6(b)).

4. Conclusion

In conclusion, we have demonstrated spin polarization detection with a side coupled quantum dot. We measured singlet–triplet levels and Zeeman split levels in a quantum dot as spin split levels. By using the Zeeman split levels and a quantum wire in magnetic fields, we confirmed the change of the tunneling signal with the change of the spin polarization. This detection scheme will operate in the zero magnetic field by using singlet–triplet levels in a quantum dot.

Acknowledgments

We thank Y. Hashimoto for technical supports. This work was supported by Grant-in-Aid for Scientific Research and Special Coordination Funds for Promoting Science and Technology.

References

[1] S.A. Wolf, D.D. Awschalom, R.A. Buhrman, J.M. Daughton, S. von Molnár, M.L. Roukes, A.Y. Chtchelkanova, D.M. Treger, Science 294 (2001) 1488.
[2] I. Žutić, J. Fabian, S. DasSarma, Rev. Modern Phys. 76 (2004) 323.
[3] E.I. Rashba, Sov. Phys. Solid State 2 (1960) 1109.
[4] Y.A. Bychkov, E.I. Rashba, J. Phys. C 17 (1984) 6039.
[5] G. Dresselhaus, Phys. Rev. 100 (1955) 580.
[6] A.A. Kiselev, K.W. Kim, Appl. Phys. Lett. 78 (2001) 775.
[7] T.P. Pareek, Phys. Rev. Lett. 92 (2004) 076601.
[8] J. Ohe, M. Yamamoto, T. Ohtsuki, J. Nitta, Phys. Rev. B 72 (2005) 041308(R).
[9] M. Eto, T. Hayashi, Y. Kurotani, J. Phys. Soc. Japan 74 (2005) 1934.
[10] G. Schmidt, D. Ferrand, L.W. Molenkamp, A.T. Filip, B.J. van Wees, Phys. Rev. B 62 (2000) R4790.
[11] T. Otsuka, E. Abe, Y. Iye, S. Katsumoto, Phys. Rev. B 79 (2009) 195313.
[12] S. Tarucha, D.G. Austing, T. Honda, R.J. van der Hage, L.P. Kouwenhoven, Phys. Rev. Lett. 77 (1996) 3613LP.
[13] K. Kobayashi, H. Aikawa, A. Sano, S. Katsumoto, Y. Iye, Phys. Rev. B 70 (2004) 035319.
[14] A.C. Johnson, C.M. Marcus, M.P. Hanson, A.C. Gossard, Phys. Rev. Lett. 93 (2004) 106803.
[15] M. Field, C.G. Smith, M. Pepper, D.A. Ritchie, J.E.F. Frost, G.A.C. Jones, D.G. Hasko, Phys. Rev. Lett. 70 (1993) 1311.
[16] E. Buks, R. Schuster, M. Heiblum, D. Mahalu, V. Umansky, Nature 391 (1998) 871.
[17] J.M. Elzerman, R. Hanson, J.S. Greidanus, L.H. Willems van Beveren, S. De Franceschi, L.M.K. Vandersypen, S. Tarucha, L.P. Kouwenhoven, Phys. Rev. B 67 (2003) 161308(R).
[18] J.M. Elzerman, R. Hanson, L.H. Willems van Beveren, L.M.K. Vandersypen, L.P. Kouwenhoven, Appl. Phys. Lett. 84 (2004) 4617.
[19] T. Otsuka, E. Abe, Y. Iye, S. Katsumoto, Appl. Phys. Lett. 93 (2008) 112111.
[20] R.M. Potok, J.A. Folk, C.M. Marcus, V. Umansky, M. Hanson, A.C. Gossard, Phys. Rev. Lett. 91 (2003) 016802.
[21] R. Hanson, B. Witkamp, L.M.K. Vandersypen, L.H.W. van Beveren, J.M. Elzerman, L.P. Kouwenhoven, Phys. Rev. Lett. 91 (2003) 196802.
[22] L.H.W. van Beveren, R. Hanson, I.T. Vink, F.H.L. Koppens, L.P. Kouwenhoven, L.M.K. Vandersypen, New J. Phys. 7 (2005) 182.
[23] B.J. van Wees, L.P. Kouwenhoven, H. van Houten, C.W.J. Beenakker, J.E. Mooij, C.T. Foxon, J.J. Harris, Phys. Rev. B 38 (1988) 3625.